Evidence for impurity-induced polar state in $Sr_{1-x}Mn_xTiO_3$ from density functional calculations

I. V. Kondakova,[1] R. O. Kuzian,[1] L. Raymond,[2] R. Hayn,[2] and V. V. Laguta[1,3]
[1]*Institute for Problems of Materials Science, NASU, Krzhizhanovskogo 3, 03180 Kiev, Ukraine*
[2]*Institut de Matériaux, Microélectronique et Nanosciences de Provence, Faculté St. Jérôme, Case 142, F-13397 Marseille Cedex 20, France*
[3]*Institute of Physics, AS CR, Cukrovarnicka 10, 16253 Prague, Czech Republic*
(Received 26 November 2008; revised manuscript received 3 March 2009; published 24 April 2009)

We have performed density functional calculations for 40- and 90-atom supercells of $SrTiO_3$ doped by manganese. We use the all-electron, full-potential local-orbital scheme. We show that Mn ion substituting for Sr occupies the off-central position. The ions of the host lattice also change their equilibrium positions when the material is doped, and the ground-state structure becomes polar. The calculated spontaneous magnetic moment of $Sr_{1-x}Mn_xTiO_3$ is 5 μ_B/Mn ion, in contrast to $SrTi_{1-x}Mn_xO_3$ which exhibits the moment of 3 μ_B/Mn. The calculation results are in accordance with the data of recent ESR and dielectric susceptibility measurements in $SrTiO_3$:Mn ceramics and support the interpretation of observed dielectric anomalies as impurity-induced transition to a polar phase caused by Mn substituting for Sr.

DOI: 10.1103/PhysRevB.79.134117 PACS number(s): 77.80.−e, 61.72.Bb, 71.20.Ps

I. INTRODUCTION

Studies of the ferroelectricity in perovskite compounds are important both from practical and fundamental points of view. The technological applications utilize their switchable macroscopic polarization and their piezoelectric properties. The rich variety of phase diagrams that they display as a function of temperature and composition makes them also attractive objects of fundamental studies.[1]

The strontium titanate $SrTiO_3$ (STO) behaves as an incipient ferroelectric in the sense that it remains paraelectric down to the lowest temperatures but has a very large static dielectric response. STO undergoes antiferrodistortive phase transition at 105 K to a tetragonal ($I4/mcm$) phase, but this transition is of nonpolar character and has little influence on the dielectric properties. The static dielectric permittivity obeys a Curie-Weiss law of the form of $\varepsilon \sim (T-T_C)^{-1}$ at temperatures above about 50 K. But instead of the divergence at $T_C \sim 36$ K the permittivity saturates at an enormous value of $\varepsilon \sim 2\times 10^4$ as T approaches zero. Due to the large polarizability of the lattice STO is very sensitive to dipole impurities which can induce various types of polar phases (dipole glass, ferroglass, and ferroelectric).

In the past few years, the Mn-doped STO has become the subject of extensive studies and discussions as Mn^{2+} ions can introduce both magnetic and electric dipoles into the system when substitute Sr^{2+} lattice ions (this will be denoted here as Mn_{Sr}^{2+}).[2,3] The expected coupling between magnetic and electric dipolar degrees of freedom in $Sr_{1-x}Mn_xTiO_3$ opens the attractive possibility to vary the magnetic properties by the application of an electric field. This one and the inverse effect may be of potential use for producing novel kinds of sensors, memory devices, and spin electronic devices.

The electric dipoles introduced by Mn impurities are manifested in appearance of the dielectric relaxation which was indeed observed in STO ceramics doped with Mn (0–15 at. %) under special conditions[4] that Mn substitutes for Sr. They exhibit a pronounced dielectric anomaly around 50 K: a diffuse maximum in the dielectric susceptibility and losses shifting to higher temperatures with increasing measurement frequency and amount of manganese.[5,6] This anomaly was attributed to a reorientational motion of dipoles formed in the host matrix due to a possible off-central position of Mn^{2+} impurity ions substituting for the Sr^{2+} ions. This interpretation was confirmed later by the detailed ESR study of the same ceramic samples $Sr_{1-x}Mn_xTiO_3$.[7] Figure 1 illustrates the main result of this work (cf. Fig. 4 of Ref. 7). Quantitative analysis of the zero-field splitting at low temperatures ($T \ll 120$ K) and the motional narrowing of the EPR linewidth at high temperatures ($T > 120$ K) agree with the supposition of the reorientational motion of Mn^{2+} ions jumping between several equivalent off-center positions. The activation energy $E_a = 86$ meV and the frequency factor

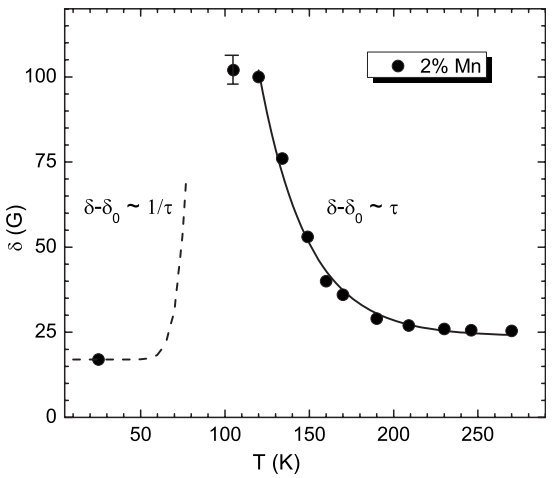

FIG. 1. Temperature dependence of Mn^{2+} ESR linewidth (half width at half maximum) in $Sr_{0.08}Mn_{0.02}TiO_3$ ceramics. In the fast motion (narrowing) regime ($T > 120$ K), the linewidth is proportional to the relaxation time of ion hopping $\tau = \tau_0 \exp(E_a/kT)$; while in the slow motion regime ($T < 80$ K) the linewidth is proportional to the rate of ion hopping $1/\tau$. Points are experimental data taken from Ref. 7; lines are numerical fits with $E_a = 86$ meV and $\tau_0 = 2 \times 10^{-14}$ s.

$1/\tau_0 \approx (1-5)\times 10^{13}$ s^{-1} for the jumping deduced from the ESR data are in agreement with those obtained by dielectric spectroscopy analysis.[5,6] In principle, earlier investigation of Mn-doped STO single crystal[8] reported very similar temperature behavior of Mn^{2+} EPR spectrum as it takes place in ceramics: the spectrum, being isotropic, undergoes strong broadening up to disappearance when the specimen is cooled to about 100 K, but upon further cooling to 4.2 K it reappears as an anisotropic spectrum. This again speaks in favor of the reorientational motion of Mn^{2+} off-centered ions that freezes at low T.

Another group of works was done on both ceramics and single-crystal samples of STO.[9–12] In particular, a low-temperature dielectric relaxation, with activation energies $E_a \sim 10-13$ and 30 meV, was reported.[10] It was ascribed to Mn^{4+} off-center ions and to Mn^{2+} ions which substitute Ti^{4+} and introduce one or two O^- holes, thus forming polaronic-type related centers. On the other hand, the relaxation with the activation energies 60–70 meV (similar to the one described in Refs. 5 and 6) was assumed to originate from inhomogeneities of Mn-doped STO ceramics in which Mn may be accumulated at the grain boundaries and/or manganese oxide enriched nanoregions.[11] However, the mechanism of this relaxation was not explained. It is the opinion of the authors of Refs. 9–12 that in their samples the Mn^{2+} ions exclusively substitute Ti^{4+} ions. The vanishing of the Mn^{2+} EPR signal at $T<120$ K was attributed to the antiferromagnetic interaction of Mn^{2+} spins in MnO nanoclusters.[12]

The brief survey above indicates that the origin of Mn induced dielectric anomalies and the structure of Mn-related centers in STO have contradicting interpretation. Therefore, further studies and arguments are necessary to prove, in particular, the equilibrium Mn position in both $Sr_{1-x}Mn_xTiO_3$ and $SrTi_{1-x}Mn_xO_3$. In this respect, the density functional theory (DFT) calculations of the total energy of $Sr_{1-x}Mn_xTiO_3$ and $SrTi_{1-x}Mn_xO_3$ systems can provide independent information about the microscopic structure of the material and can supplement the experimental data presented above by new arguments.

Previous DFT calculations of STO were mainly devoted to the consideration of structural instabilities and phonon spectra. The results indicate that the ferroelectric and antiferrodistortive instabilities depend very sensitively on the volume, the applied density functional, and other details of the calculation (see Refs. 13–17 and, most recent, Refs. 18–20 with references therein). Note that the energy difference between the cubic and the ferroelectric phases is a few meV, the total energy of every phase being dozens of thousands eV. Therefore, in contrast to $BaTiO_3$ and to many other perovskites, it is particularly hard to predict whether STO is unstable toward a ferroelectric distortion or not.[20] This question seems to be on the verge of the precision accessible for modern DFT calculations.

The defects in STO are modeled within DFT by the supercell method. STO:Fe was considered in Ref. 21; STO:Ca in Ref. 22. For another incipient ferroelectric $KTaO_3$ (KTO), which is similar to STO in many respects, the off centrality of impurity ions and their reorientational dynamics were considered in Ref. 23 for KTO: Mn and Ca, and in Ref. 24 for KTO:Li. These investigations showed that a DFT calculation is reliable to predict an energy gain due to an impurity shift, at least when this gain is on the order of 100 meV.

In this paper, we present results of density functional calculations of the total energy of $Sr_{1-x}Mn_xTiO_3$ and $SrTi_{1-x}Mn_xO_3$ systems within the local spin-density approximation (LSDA). In particular, we show that the equilibrium position of the Mn ion substituting for Sr is shifted from the position of the host ion. Thus, the Mn ion forms a dipole impurity and may be responsible for the dielectric anomalies observed in STO:Mn systems.

II. METHODS

The DFT calculations were performed within the LSDA. We have used the all-electron full-potential local-orbital (FPLO) code (version 7.00–28) (Ref. 25) with the standard double numerical basis. The method implemented in the FPLO code retains the simplicity and physical transparency of the linear combination of atomic orbital (LCAO) method, but it is free from the well-known defaults of the LCAO. The idea is to add an artificial confining potential $\propto r^4$ to the potential of the nucleus in order to make the basis functions more localized than the atomic orbitals.[26] Due to thorough optimization the FPLO code combines the high precision with the efficiency of the calculations. FPLO makes it possible to perform all-electron calculations for the supercells containing up to 100 atoms. Another advantage of the code is the possibility to analyze the resulting electron density in terms of occupation numbers of local orbitals, the latter being characterized by nlm quantum numbers closely related to the well-known classification of atomic orbitals.[25] Such values as ionic charges and local densities of states are less ambiguous than in codes using the division of space on spheres and interspherical regions.

Starting from the seventh version of the code, the choice of a basis is automatized so the input data include only positions and charges of nuclei in a unit cell of a crystal, a **k**-mesh subdivision, and a version of the exchange-correlation potential. In our scalar relativistic calculations, the exchange and correlation potential of Perdew and Wang[27] was employed.

The **k**-mesh subdivision gives the subdivision of the Brillouin zone along the three axes from which the k-space integration mesh is constructed. We have used the default value $12\times12\times12$ for pure STO, $6\times6\times6$ for 40-, and $2\times2\times2$ for 90-atom STO supercells correspondingly.

The experimental data give strong evidence for the off centrality of Mn_{Sr}^{2+} both in the cubic and in the tetragonal phase. In this work, we have considered structure deviations from cubic phase only within the tetragonal space group (99) $P4mm$. We thus postpone the account of the structural changes caused by the antiferrodistorsive transition to the future work.

In view of the experimental observation that the lattice parameter a of $Sr_{1-x}Mn_xTiO_3$ weakly depends on x($a \approx 3.905\,98-0.026\,61x$ Å),[4] we have performed all supercell calculations at fixed parameter $a=3.9$ Å.

III. RESULTS AND DISCUSSIONS

A. $SrTiO_3$

Within the above approximations, we have first performed calculations for pure STO. The local-density approximation

TABLE I. The experimental (extrapolated to 0 K) and calculated values of the lattice parameter and bulk modulus for the cubic phase of $SrTiO_3$.

	Lattice parameter (Å)	Bulk modulus (GPa)
Present	3.863	183
Ref. 20[a]	3.863	198
Ref. 15[b]	3.922	190
Ref. 14[a]	3.865	200
Exp., Ref. 28	3.900	
Exp., Ref. 29		180

[a]Pseudopotential.
[b]Linearized augmented plane waves.

(LDA) equilibrium lattice constants and bulk modulus are compared with previous calculations and experiment in Table I. One can see that the results of our calculations are in good agreement with the results obtained by other codes, and those deviations from experimental values are within the limits of the LDA itself.

Recently, the FPLO code was successfully applied for the calculation of the electric field gradient on oxygen site of $SrTiO_3$ and $BaTiO_3$. The results that will be published elsewhere[30] are in good agreement with the experiment and linearized augmented planewave (LAPW) calculations.[31]

As we have mentioned in Sec. I, the ferroelectric instability for the STO strongly depends on the lattice parameter. In our calculation, STO appears to be stable against the spontaneous Ti displacement along the [001] direction for the experimental lattice parameter $a=3.9$ Å. Figure 2 shows the total energy dependence on the value of the displacement for various lattice parameter values, with other ions being fixed at the equilibrium positions in the cubic phase. We see that an increase in lattice parameter by about 3% leads to a break of the cubic symmetry in favor of Ti sublattice shift.

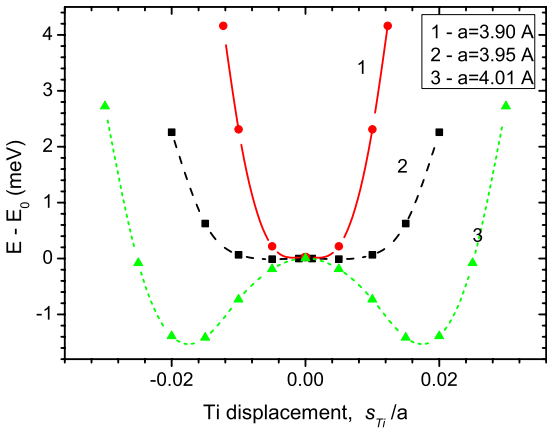

FIG. 2. (Color online) The total energy dependence $E(s_{Ti})-E_0[E_0\equiv E(0)]$ on the value of Ti displacement along the [001] direction.

B. $Sr_{1-x}Mn_xTiO_3$

In order to model the STO:Mn, we have constructed the $2\times2\times2$ and $3\times3\times2$ STO supercells with one Mn ion substituting for Sr site. Thus, we have obtained $Sr_7MnTi_8O_{24}$ and $Sr_{17}MnTi_{18}O_{54}$ supercells, which model $Sr_{1-x}Mn_xTiO_3$ for $x=1/8=12.5\%$ and $x=1/18\approx5.6\%$. For $Sr_7MnTi_8O_{24}$ supercell and the space group (99) $P4mm$, there are 14 Wyckoff positions, which are indicated in Table II. In order to take into account the paramagnetic nature of Mn ions, we have made the spin-polarized calculations within LSDA.

Figure 3 shows the dependence of the total energy (per Mn ion) on the value of Mn shift in the [001] direction, $E(s)$. For comparison, we give also the curve for $x=100\%$ (i.e., $MnTiO_3$ compound in the artificial perovskite structure). We see that the curves for $x=1/8$ and $x=1/18$ almost coincide. The minimum of the total energy for both supercells corresponds to the Mn shift $s_0\approx0.64$ Å. So, we may assume that for an isolated Mn impurity (i.e., for $x\to0$ and vanishing

TABLE II. Fractional atomic coordinates x,y,z of the atoms of tetragonal $Sr_7MnTi_8O_{24}$ supercell [space group (99) $P4mm$] and those charges (in the units of fundamental charge) $Q(s)$ for two values of Mn shift s.

No.	Ion	$x/2a$	$y/2a$	$z/2a$	$Q(0)$	$Q(s_0)$
1	Mn	0.00	0.00	s	1.287	1.268
2	Sr	0.00	0.00	0.50	1.555	1.542
3	Sr	0.50	0.00	0.00	1.555	1.559
4	Sr	0.50	0.00	0.50	1.548	1.545
5	Sr	0.50	0.50	0.00	1.548	1.545
6	Sr	0.50	0.50	0.50	1.550	1.551
7	Ti	0.25	0.25	−0.25	1.960	1.972
8	Ti	0.25	0.25	0.25	1.960	1.942
9	O	0.25	0.00	−0.25	−1.150	−1.141
10	O	0.25	0.00	0.25	−1.150	−1.155
11	O	0.25	0.25	0.00	−1.150	−1.143
12	O	0.25	0.25	0.50	−1.169	−1.168
13	O	0.25	0.50	−0.25	−1.169	−1.171
14	O	0.25	0.50	0.25	−1.169	−1.165

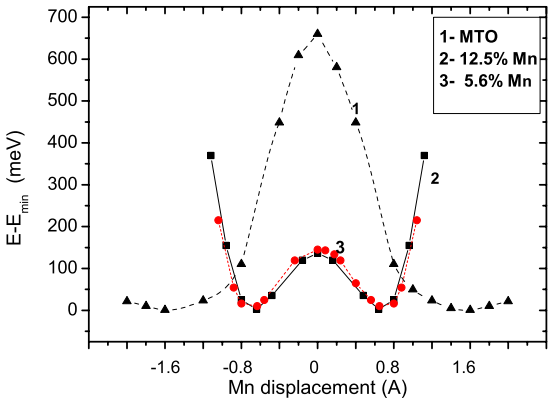

FIG. 3. (Color online) The dependence of the total energy (per Mn ion) $E(s)-E_{\min}[E_{\min}\equiv E(s_0)]$ on the value of Mn shift in the [001] direction

Mn-Mn interaction, which is inevitable in our supercells) the value of the shift will be close to this value. This result clearly indicates that manganese ion substituting Sr occupies the off-central position and creates reorientational dipole. The energy difference $\Delta E=E(0)-E(s_0)\approx 133$ meV gives the order of magnitude of the energetic barrier for the reorientational motion. It is clear that in the cubic phase there are six equivalent off-central positions for the Mn ion that is shifted along the [001] direction. Two of them are shown in Fig. 3. The reorientation of a dipole from $\mathbf{r}_0=(0,0,s_0)$ to $-\mathbf{r}_0$ may go via an intermediate $\mathbf{r}_1=(0,s_0,0)$ position, which is separated from $\mathbf{r}_0$ by a saddle point $\mathbf{r}_s$ along the [110] direction with the energy $E(\mathbf{r}_s)<E(\mathbf{0})$. So, the agreement between ΔE and the experimentally found barrier height $E_a=91-99$ meV [Arrhenius law fit of the temperature dependence of the relaxation time for $x=3\ldots15\%$ (Ref. 32)] and $E_a=86$ meV [ESR, $x=0.5,2\%$ (Ref. 7)] may be regarded as reasonable.

It is clear that the Mn displacement will result in shifts of surrounding ions. The determination of the fully relaxed structure is out of the scope of the present paper. We expect that the distortions around an off-centered Mn will be similar to the distortions around the Li impurity in $KTaO_3$ (KTL) (see Fig. 2 in Ref. 24). In the KTL, the oxygen ion in tenth Wyckoff position (O_{10}) exhibits the largest shift, which is about 12% of the Li shift; the shifts of the other ions do not

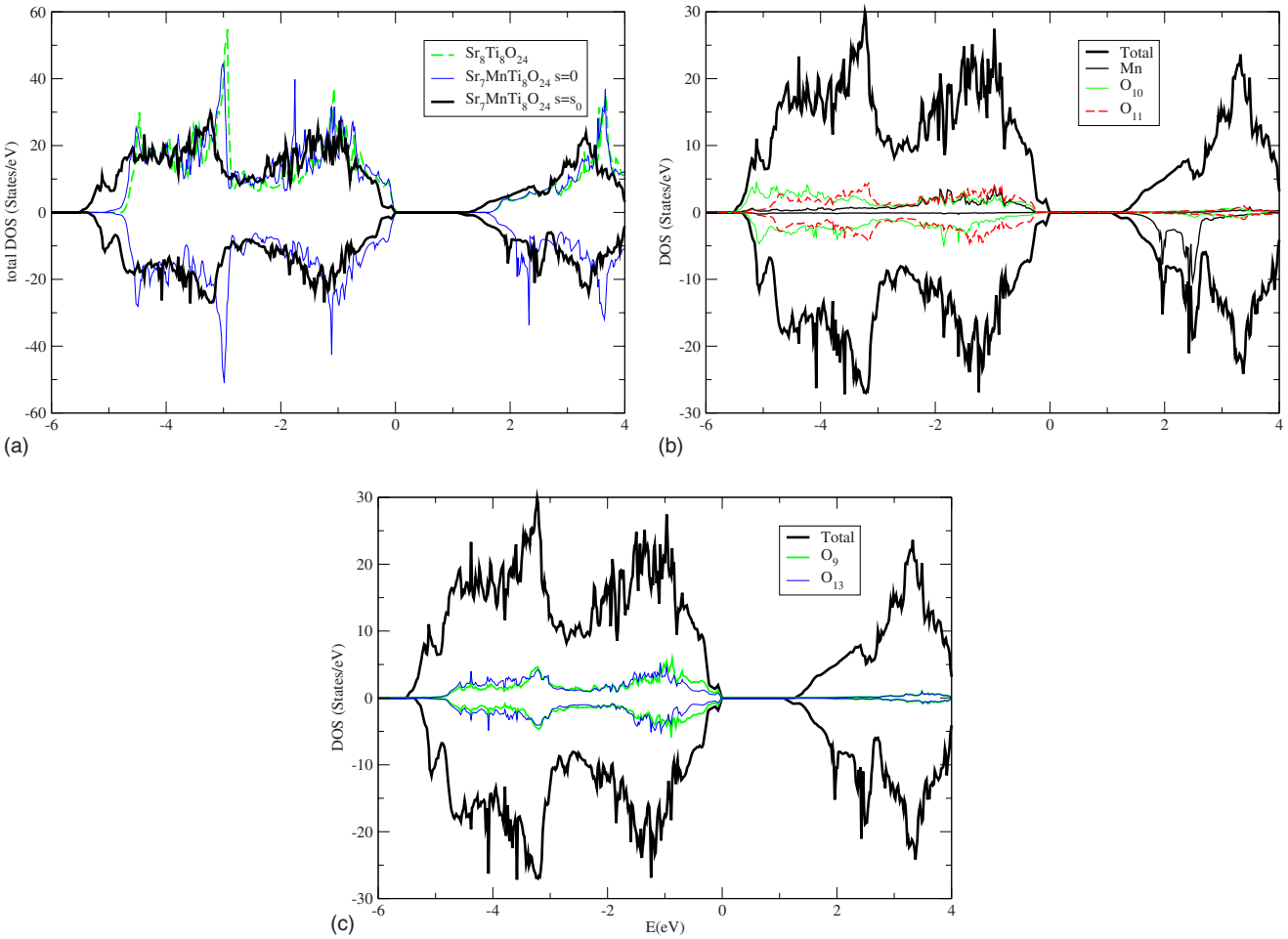

FIG. 4. (Color online) (a) DOS for the $Sr_7MnTi_8O_{24}$ supercell. The Mn shift in the [001] direction corresponds to the minimum of the energy in Fig. 3. Positive (negative) values correspond to the majority (minority) spin projection. Total DOSs for the unshifted Mn and for the pure $SrTiO_3$ are given for comparison. (b) Sort projected (i.e., the sum of all contributions of all sites belonging to the same Wyckoff position) DOS for the Mn and typical O sites coupled with Mn. (c) Sort projected DOS for O sites laying in XY plane left behind ($s_0+a/2$ below) the Mn ion.

exceed 6% of Li shift value. The oxygen relaxation leads to an increase in the total energy gain and favors a larger Li shift from the central position. In order to check if the same tendency is exhibited in our case, we have shifted O_{10} by the value $\Delta x/2a=0.03$ and $\Delta z/2a=0.05$. Then the minimum of the total energy is $\Delta E_{\text{tot}} \approx 82$ meV lower and occurs at slightly larger Mn shift $s \approx 0.66$ Å than for the unshifted oxygens (cf. Fig. 3 in Ref. 24).

In order to see the changes in the electronic structure caused by the Mn shift, we have calculated the total and the sort projected densities of states (DOS) for the $Sr_7MnTi_8O_{24}$ supercell. They are shown in Fig. 4. Figure 4(a) shows the changes in the total DOS when Mn shifts from the central position; the total DOS for STO supercell is also shown. We see that the substitution of one Mn for Sr does not change much the total DOS of the 40-atom supercell provided that Mn occupies the central position. The DOS, which corresponds to the minimum of the total energy with respect to the Mn shift, is substantially different: the valence band becomes 0.5 eV broader, a large part of states move to lower energy, and the rest of states form a new structure within 0.2 eV below the Fermi energy ($E_F=0$). Comparison of sort projected densities of states shown in Figs. 4(b) and 4(c) tells us that the top of the valence band is formed by states which belongs to oxygen ions in 9th and 13th Wyckoff positions. These O sites are situated in the XY plane, which is $s_0+a/2$ below the Mn ion. The states of other oxygens as well as Mn majority spin band lie below −0.2 eV. The last two columns of the Table II show the charge redistribution resulting in the Mn shift. We see that most of ion charges diminish. This fact together with the increase in the valence band width point to the increase in states mixing and an enhancement of covalence character of metal-oxygen bonds accompanied to the Mn shift.

It is tempting to ascribe the Mn off centrality to the band-energy gain which occurs due to the DOS redistribution which accompanies the Mn shift. In fact, the gain in the band energy is more than 5 eV, and the gain in the total energy is only 3% of this value (see Fig. 5).

So, a thorough analysis of other contributions to the total energy is needed in order to name the main reason for the Mn ion to shift. In this context, it is worth recalling the paper of Foulkes and Haydock[33] where they argued that the total energy functional may be approximately rewritten as a sum of band energy and a sum of short-range pairwise interatomic repulsion potentials. This approach qualitatively justifies the concept of ionic radius and empirical observation that an impurity ion becomes off centered when it substitutes a host ion of larger radius. For perovskites, evidently, the long-range Coulomb interactions also contribute to the total energy. The quantitative consideration of the mechanism of Mn_{Sr} instability in the STO will be the subject of a separate investigation.

It is instructive to note a substantial dependence of the band energy of the core states on the Mn shift s that is shown in the Fig. 5. That justifies the use of the all-electron method in the DFT calculation.

In a solid with ionic or polar covalent bonding, an isovalent impurity with a charge Z displaced from the site of the substituted ion at a vector $\mathbf{s}$ may be regarded as an addition

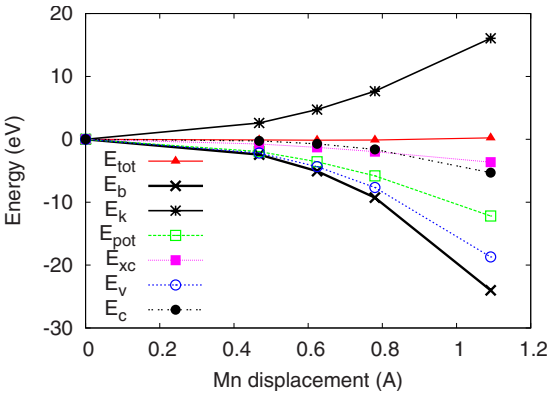

FIG. 5. (Color online) The band energy $E_b(s)-E_b(0)(\times)$, which is the sum of core $[E_c(s)-E_c(0)$, filled circles] and valence $[E_v(s)-E_v(0)$, circles] energies, and various contributions to the total energy $E_{\text{tot}}(s)-E_{\text{tot}}(0)$ (filled triangles): kinetic energy $E_k(s)-E_k(0)(*)$, potential energy $E_{\text{pot}}(s)-E_{\text{pot}}(0)$ (squares), and exchange-correlation energy $E_{\text{xc}}(s)-E_{\text{xc}}(0)$ (filled squares) as functions of Mn displacement s.

of a dipole $\mathbf{d}=Z\mathbf{s}$ to the ideal lattice. The dipole polarizes the lattice, with the size of the polarized region being on the order of the correlation length of the transverse optic phonon mode. The polarization acts on the adjacent dipole impurities. This dipole-dipole interaction mediated by the polarizable lattice[34] induces the ferroelectric phase in the crystal if the average distance between impurities is less than the correlation radius.

Figure 6 shows the total energy in dependence on the Ti sublattice shift. The Ti sublattice shifts along the [001] direction for the $Sr_7MnTi_8O_{24}$ and $Sr_{17}MnTi_{18}O_{54}$ supercells, with the Mn sublattice being displaced in the same direction by s_0. We see that in contrast to the pure STO (cf. Fig. 2) the minimum of the energy corresponds to the nonzero shift $s_{\text{Ti}}(x)$ of the sublattice. The additional energy gain is 15 and 7.6 meV for $x=1/8, 1/18$ correspondingly. The value of the shift is roughly proportional to the zero-temperature limit of

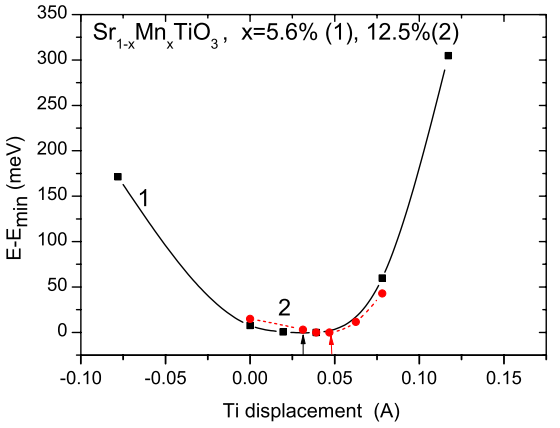

FIG. 6. (Color online) The total energy (per supercell) dependence $E(s_{\text{Ti}})-E_{\text{min}}$ on Ti sublattice shift along the [001] direction for two Mn concentrations. The positions of energy minima E_{min} are indicated by arrows for each concentration. The Mn ions are shifted in the same direction by the value s_0 that corresponds to the minimum of the energy in Fig. 3.

the spontaneous polarization of the lattice. We see that the larger Mn concentration induces larger polarization. This behavior agrees with the results of the hysteresis loop (polarization vs field) measurements.[6,32]

Let us recall that the modeling of defects by the supercell method disregards the disorder in the lattice. So, the ferroelectric ground state of our model system, with regular arrangement of Mn impurities, means only that Mn polarizes the surrounding lattice. In a real material, the randomness of Mn_{Sr} positions in the lattice may suppress the occurrence of a uniform ferroelectric state but may lead to a polar glass state. We have checked also that Mn shift induces a small tetragonal strain $c/a \approx 1.002$ of the lattice, with the additional energy gain being about 1 meV for $Sr_7MnTi_8O_{24}$.

For both supercells the converged solution exhibits a magnetic moment of 5 μ_B per unit cell containing one Mn ion. The Mn magnetic moment is about 4.8 μ_B; the polarization of other ions does not exceed 0.03 μ_B. So, the LSDA evidences that the paramagnetic center associated with Mn_{Sr} impurity possesses the spin value of 5/2. The Mn-projected DOS shown in Fig. 4(b) indicates a full polarization of Mn *d* shell, which is manifested by the absence of minority states in the valence band and of majority states in the conduction band.

We have also performed the LSDA calculations for $Sr_{18}Ti_{17}MnO_{54}$ supercell, which model $SrTi_{1-x}Mn_xO_3$ for $x = 1/18$. The magnetic moment is then 3 μ_B per unit cell; the Mn moment is approximately 2.7 μ_B. So, the spin value of the paramagnetic center Mn_{Ti} should be 3/2 in this case. Hence, our calculations support the interpretation of ESR experiments (see Ref. 7 and references therein) where the Mn^{2+} and $S=5/2$ paramagnetic centers are ascribed to Mn_{Sr} impurity, while Mn^{4+} and $S=3/2$ are ascribed to Mn_{Ti}.

IV. SUMMARY

We have modeled the Mn impurities in strontium titanate by means of 40- and 90-atom supercells with one metal ion substituted by the Mn ion. The total energy LSDA calculations unambiguously show that Mn substituting for Sr occupies the off-central position. Thus, the Mn_{Sr} possess simultaneously the dipole and magnetic moments, with its spin value being $S=5/2$. The barrier height for the reorientational motion estimated from the LSDA calculation is in accordance with that obtained by dielectric spectroscopy and ESR analysis. The Mn substituting for Ti ion possess the spin value of $S=3/2$ and cannot be related with the Mn^{2+} center which exhibits the zero-field splitting and motional narrowing at temperatures $T>120$ K. We conclude that LSDA supercell calculation supports the explanation of dielectric anomalies in $SrTiO_3$:Mn ceramics as being due to the correlated motion of reorientable Mn_{Sr} dipole impurities interacting via the highly polarizable host crystal.

ACKNOWLEDGMENTS

The authors thank the "DNIPRO" (Contract No. 14182XB) program for financial support and the IFW Dresden (Germany) for use of their computer facilities. The Institutional Research Plan (Contract No. AVOZ10100521) is acknowledged.

[1] M. E. Lines and A. M. Glass, *Principles and Applications of Ferroelectrics and Related Materials* (Clarendon, Oxford, 1977).
[2] W. Kleemann, V. V. Shvartsman, S. Bedanta, P. Borisov, A. Tkach, and P. M. Vilarinho, J. Phys.: Condens. Matter **20**, 434216 (2008).
[3] V. V. Shvartsman, S. Bedanta, P. Borisov, W. Kleemann, A. Tkach, and P. M. Vilarinho, Phys. Rev. Lett. **101**, 165704 (2008).
[4] A. Tkach, P. M. Vilarinho, and A. L. Kholkin, Acta Mater. **53**, 5061 (2005).
[5] A. Tkach, P. M. Vilarinho, and A. L. Kholkin, Appl. Phys. Lett. **86**, 172902 (2005).
[6] A. Tkach, P. M. Vilarinho, A. L. Kholkin, A. Pashkin, S. Veljko, and J. Petzelt, Phys. Rev. B **73**, 104113 (2006).
[7] V. V. Laguta, I. V. Kondakova, I. P. Bykov, M. D. Glinchuk, A. Tkach, P. M. Vilarinho, and L. Jastrabik, Phys. Rev. B **76**, 054104 (2007).
[8] R. A. Serway, W. Berlinger, K. A. Muller, and R. W. Collins, Phys. Rev. B **16**, 4761 (1977).
[9] V. V. Lemanov, E. P. Smirnova, A. V. Sotnikov, and M. Weihnacht, Phys. Solid State **46**, 1442 (2004).
[10] V. V. Lemanov, A. V. Sotnikov, E. P. Smirnova, and M. Weihnacht, J. Appl. Phys. **98**, 056102 (2005).
[11] M. Savinov, V. A. Trepakov, P. P. Syrnikov, V. Železný, J. Pokorný, A. Dejneka, L. Jastrabík, and P. Galinetto, J. Phys.: Condens. Matter **20**, 095221 (2008).
[12] A. G. Badalyan, C. B. Azzoni, P. Galinetto, M. C. Mozzati, V. A. Trepakov, M. Savinov, A. Deyneka, L. Jastrabik, and J. Rosa, J. Phys.: Conf. Ser. **93**, 012012 (2007).
[13] W. Zhong and D. Vanderbilt, Phys. Rev. Lett. **74**, 2587 (1995).
[14] R. D. King-Smith and D. Vanderbilt, Phys. Rev. B **49**, 5828 (1994).
[15] C. LaSota, C. Z. Wang, R. Yu, and H. Krakauer, Ferroelectrics **194**, 109 (1997).
[16] N. Sai and D. Vanderbilt, Phys. Rev. B **62**, 13942 (2000).
[17] Zh. Wu, R. E. Cohen, and D. J. Singh, Phys. Rev. B **70**, 104112 (2004).
[18] E. Heifets, E. Kotomin, and V. A. Trepakov, J. Phys.: Condens. Matter **18**, 4845 (2006).
[19] N. Choudhury, E. J. Walter, A. I. Kolesnikov, and C.-K. Loong, Phys. Rev. B **77**, 134111 (2008).
[20] R. Wahl, D. Vogtenhuber, and G. Kresse, Phys. Rev. B **78**, 104116 (2008).
[21] R. A. Evarestov, S. Piskunov, E. A. Kotomin, and G. Borstel, Phys. Rev. B **67**, 064101 (2003).
[22] G. Geneste and J.-M. Kiat, Phys. Rev. B **77**, 174101 (2008).
[23] K. Leung, Phys. Rev. B **63**, 134415 (2001).
[24] S. A. Prosandeev, E. Cockayne, and B. P. Burton, Phys. Rev. B **68**, 014120 (2003).

[25] Improved version of the original FPLO code by K. Koepernik and H. Eschrig, Phys. Rev. B **59**, 1743 (1999), FPLO-7, 00–28 (http://www.FPLO.de).
[26] H. Eschrig, *Optimized LCAO Method and the Electronic Structure of Extended Systems* (Springer, Berlin, 1989).
[27] J. P. Perdew and Y. Wang, Phys. Rev. B **45**, 13244 (1992).
[28] Y. A. Abramov, V. G. Tsirelson, V. E. Zavodnik, S. A. Ivanov and I. D. Brown, Acta Crystallogr. B **51**, 942 (1995).
[29] *Ferroelectrics and Related Substances*, edited by K. H. Hellwege and A. M. Hellwege, Landolt-Börnstein, New Series, Group III, Vol. 3 (Springer-Verlag, Berlin, 1969).
[30] K. Koch, R. O. Kuzian, K. Koepernik, I. V. Kondakova, and H. Rosner, arXiv:0903.4015v1 (unpublished).
[31] R. Blinc, V. V. Laguta, B. Zalar, M. Itoh, and H. Krakauer, J. Phys.: Condens. Matter **20**, 085204 (2008).
[32] A. Tkach, Ph. D. thesis, University of Aveiro, 2005.
[33] W. M. C. Foulkes and R. Haydock, Phys. Rev. B **39**, 12520 (1989).
[34] B. E. Vugmeister and M. D. Glinchuk, Rev. Mod. Phys. **62**, 993 (1990).